Available online at www.sciencedirect.com
SCIENCE DIRECT®
Journal of Solid State Chemistry 178 (2005) 3529–3540
JOURNAL OF SOLID STATE CHEMISTRY
www.elsevier.com/locate/jssc

Syntheses and crystal structures of several novel alkylammonium iodobismuthate materials containing the 1,3-bis-(4-piperidinium)propane cation

Andrea M. Goforth[a], LeRoy Peterson Jr.[b], Mark D. Smith[a], Hans-Conrad zur Loye[a,*]

[a]*Department of Chemistry and Biochemistry, Graduate Sciences Research Center, The University of South Carolina, 631 Sumter Street, Columbia, SC 29208, USA*

[b]*Department of Chemistry, Francis Marion University, Florence, SC 29501, USA*

Received 28 June 2005; received in revised form 25 August 2005; accepted 6 September 2005
Available online 17 October 2005

Abstract

The inorganic–organic salts $(H_2TMDP)_3(Bi_2I_9)_2$ (**1**), $(H_2TMDP)_2(Bi_4I_{16})\cdot 2EtOH$ (**2**), $(H_2TMDP)_2(Bi_6I_{22})\cdot 2EtOH$ (**3**), and $(H_2TMDP)_2(Bi_6I_{22})$ (**4**) were synthesized and structurally characterized from the solvothermal reaction of 1,3-bis-(4-piperidyl)propane (TMDP) and BiI_3 by adjusting the relative ratio of the reactants. The anions of the compounds consist of 2 (**1**), 4 (**2**), or 6 (**3** and **4**) BiI_6 polyhedra, which are joined by face- (**1**) or edge-sharing (**2**–**4**) to form discrete anions. The size of the discrete anion, in terms of the number of connected polyhedra, is observed to increase as the ratio of BiI_3 to TMDP is increased. A related compound $(H_2TMDP)(Bi_3I_{11})\cdot(H_2O)$ (**5**) was synthesized and structurally characterized using the same two reactants in the presence of HF. The anion of **5** is polymeric rather than discrete, with a trioctahedral repeat unit.

Keywords: Crystal structure; Bismuth iodide; Halobismuthate; Iodobismuthate

1. Introduction

The chemistry of the main group metal halides has been widely explored for several decades owing to the interesting physical properties that have often been observed in such systems including luminescence, semiconductivity, and second-order non-linear optical activity [1–5]. To date, numerous metal–halide systems involving Sn, Pb, Sb, Bi, and Te have been synthesized and structurally characterized [1–10]. In general, these systems contain a complex metal–halide anion in which MX_n (M = metal, X = halide) coordination polyhedra are linked by corner-, edge-, or face-sharing. Charge balance in these systems is typically provided by an organic cation, although it has been demonstrated that inorganic cations or metal coordination cations are also viable charge-balancing counter-ions [11–14].

In addition to the promising physical properties observed in this family of materials, tremendous structural diversity is also encountered—particularly with respect to the dimensionality, size, and connectivity of the anionic component. The anionic metal–halide species has been observed to range in dimensionality from two-dimensional (2-D) or one-dimensional (1-D) polymeric anions to discrete anions of various sizes. The size and dimensionality of the anionic component is tied to the specific reaction conditions employed, particularly the identity of the metal and the size, charge density, and relative concentration of the cation. Because of the ability to influence the dimensionality and size of the anionic component, size- and dimensionality-dependent physical properties (i.e., quantum confinement effects) may be observed in such systems.

The bismuth(III) trihalides (BiX_3) have been employed in the synthesis of numerous metal–halide materials owing to the ability of Bi^{3+} to function as a good Lewis acid and a strong halide ion acceptor [15,16]. Typically, BiX_3 is

*Corresponding author. Fax: +1 803 777 8508.
E-mail addresses: zurloye@mail.chem.sc.edu, jssc@mail.chem.sc.edu (H.-C. zur Loye).

0022-4596/$ - see front matter © 2005 Elsevier Inc. All rights reserved.
doi:10.1016/j.jssc.2005.09.010

reacted in the presence of a cation source and a halide ion source to produce the halobismuthate compound, where formation of the anionic species is thought to occur via uptake of X^- by neutral BiX_3. X^- anions may be supplied to Bi^{3+} either by the cationic reagent, by a haloacid (H*X*), or by BiX_3 itself [9,17,18]. With respect to the cations, alkylamines, or alkylammonium halides have been employed as cationic reagents by us and others with great success [1,10,19,20]. In cases where an alkylamine is employed as the cationic reagent, protonation of the alkylamine during the solvothermal synthesis is observed.

This paper describes the solvothermal syntheses and X-ray structural analyses of a series of alkylammonium iodobismuthate materials synthesized from BiI_3 and the alkylamine 1,3-bis-(4-piperidyl)propane (TMDP). The size dependence of the anionic component on the relative concentration of reagents is examined along with the influence of additional reagents (i.e., HF) on the nature of the anion formed.

2. Experimental

2.1. Materials

BiI_3 (Alfa Aesar, 95%), trimethylenedipiperidine monohydrate ($TMDP \cdot H_2O$, also called 1,3-bis(4-piperidyl)propane monohydrate, Lancaster, 98%), ethanol (AAPER, 100%), and aqueous HF (Fisher, 49% solution) were purchased from commercial sources and used as received.

2.2. Synthesis of $(H_2TMDP)_3(Bi_2I_9)_2$ (*1*)

BiI_3 (50 mg, 0.08 mmol), $TMDP \cdot H_2O$ (13 mg, 0.06 mmol), and 6 mL absolute ethanol were added to a 23 mL Teflon lined autoclave, and the contents were stirred for several minutes prior to sealing the vessel. The autoclave was heated to 140 °C at a rate of 1 °C/min and held at that temperature for 24 h. The autoclave was subsequently cooled at 1 °C/min to 60 °C where the temperature was held for 6 h. The vessel was finally cooled to room temperature at a rate of 1 °C/min. Air-sensitive, red-orange single crystals and a red-orange polycrystalline material were isolated from the reaction. A suitable single crystal was selected for the structural determination. Crystals of **1** lose crystallinity upon removal from the mother liquor. Because of this, powder X-ray diffraction analysis cannot be used to verify that the polycrystalline material is the same as the single crystals, and the product yield was not calculated.

2.3. Synthesis of $(H_2TMDP)_2(Bi_4I_{16}) \cdot 2EtOH$ (*2*)

The synthesis is the same as that used to prepare compound **1** except that 6.5 mg $TMDP \cdot H_2O$ (0.03 mmol) were used instead of 13 mg $TMDP \cdot H_2O$ (0.06 mmol).

Air-sensitive, red-orange single crystals and red-orange polycrystalline material were isolated from the reaction, and a suitable single crystal was selected for the structural determination. Crystals of **2** quickly turn opaque upon removal from the mother liquor. Thus, the identity of the polycrystalline material could not be confirmed by powder X-ray diffraction, and the product yield was not calculated.

2.4. Synthesis of $(H_2TMDP)_2(Bi_6I_{22}) \cdot 2EtOH$ (*3*) and $(H_2TMDP)_2(Bi_6I_{22})$ (*4*)

$(H_2TMDP)_2(Bi_6I_{22}) \cdot 2EtOH$ was prepared from 100 mg BiI_3 (0.16 mmol) and a trace amount of $TMDP \cdot H_2O$. Trace amounts of the diamine (TMDP) were delivered as follows: 620 mg $TMDP \cdot H_2O$ were placed in a Teflon lined, stainless-steel autoclave and covered with 6 mL of absolute ethanol. The autoclave was then sealed and heated to 160 °C at 1 °C/min. This temperature was maintained for 48 h before cooling the autoclave to room temperature at a rate of 1 °C/min. The autoclave was then opened, rinsed out with deionized water, and wiped dry. At this stage, only TMDP molecules hydrogen bonded to the PTFE liner remained in the reaction vessel. Once dry, 100 mg BiI_3 (0.16 mmol) and 6 mL of absolute ethanol were added to the Teflon liner, which was then sealed and heated to 140 °C at a heating rate of 1 °C/min. The reaction vessel was kept at 140 °C for 2 days before it was cooled to 70 °C at a rate of 0.5 °C/min. The autoclave was subsequently kept at 70 °C for 6 h before it was cooled to room temperature at a rate of 0.5 °C/min. Air-sensitive, red crystals and red polycrystalline material were obtained. A suitable single crystal was selected for the X-ray crystallographic analysis. Analysis of multiple crystals from the same batch revealed that two different crystalline products were present. These two pseudo-polymorphic compounds, $(H_2TMDP)_2(Bi_6I_{22}) \cdot 2EtOH$ (**3**) and $(H_2TMDP)_2(Bi_6I_{22})$ (**4**), differ in their constitution only with respect to the presence of ethanol molecules of crystallization in **3** but not in **4**. The yield of single crystals for the reaction producing **3** and **4** was low, with the majority of the solid product being the unidentifiable red polycrystalline material. Because of the mixed nature of the reaction product, the reaction yield was not estimated or calculated. Despite the low yield of the single crystalline phases and despite the fact that the precise concentration of the cation source cannot be determined, the synthesis of **3** and **4** involving the release of trace amounts of the ammonium cation from the Teflon reaction vessel is reproducible. In fact, it is a known phenomenon that amines will hydrogen bond to Teflon reaction vessels and that they may become reagents in subsequent syntheses using the same vessel. Consequently, precaution must be taken against cross-contamination of reactions when amines are used as reagents.

2.5. Synthesis of $(H_2TMDP)(Bi_3I_{11}) \cdot H_2O$ (*5*)

BiI_3 (100 mg, 0.16 mmol), $TMDP \cdot H_2O$ (29 mg, 0.13 mmol), 5 mL absolute ethanol, and 1 mL of 49% aqueous HF were placed in a Teflon lined autoclave and

stirred for several minutes prior to sealing. The autoclave was then heated at a rate of 0.5 °C/min to 180 °C where the temperature was maintained for 3 days before the vessel was cooled to room temperature at a rate of 0.2 °C/min. After opening the autoclave, the bright orange supernatant was removed and replaced with fresh absolute ethanol. Large red, bar-shaped crystals and thin, yellow needle crystals were observed. The yellow, needle-like crystals were brittle, thin, and poor X-ray scatterers. A suitable crystal of the red crystalline phase, $(H_2TMDP)(Bi_3I_{11}) \cdot H_2O$, was selected for X-ray crystallography and solved. Due to the difficulty in manual separation of the two phases, product yields were not calculated.

2.6. Single-crystal structure determinations

Suitable single crystals of compounds **1**–**5** were selected and mounted on the end of thin glass fibers using an inert

Table 1
Crystal data and structure refinement summary for **1–5**

Compound	**1**	**2**	**3**
CCDC deposit no.	271581	271582	271583
Empirical formula	$C_{39}H_{84}Bi_4I_{18}N_6$	$C_{30}H_{68}Bi_4I_{16}N_4O_2$	$C_{30}H_{68}Bi_6I_{22}N_4O_2$
Formula weight	3757.24	3383.20	4562.56
Temperature	150.0(2) K	150.0(2) K	150.0(2) K
Crystal system	Triclinic	Triclinic	Triclinic
Space group	*P*-1	*P*-1	*P*-1
a (Å)	11.9736(6)	11.3210(5)	11.7183(6)
b (Å)	12.9093(7)	12.3533(6)	12.0560(7)
c (Å)	14.7602(8)	14.1219(7)	15.7874(8)
α°	76.8640(10)	72.5250(10)	89.1380(10)
β°	77.5740(10)	74.1120(10)	81.9110(10)
γ°	70.1210(10)	71.4670(10)	69.9420(10)
Volume (Å^3)	2065.58(19)	1751.07(14)	2072.93(19)
Z	1	1	1
Density (calculated, Mg/m^3)	3.020	3.208	3.655
Absorption coefficient (mm^{-1})	15.248	17.099	20.907
F(000)	1646	1472	1956
Crystal size	$0.20 \times 0.10 \times 0.04\,mm^3$	$0.20 \times 0.08 \times 0.02\,mm^3$	$0.16 \times 0.08 \times 0.06\,mm^3$
Reflections collected	14653	16116	17137
Independent reflections	7254 [$R_{int} = 0.0420$]	7149 [$R_{int} = 0.0470$]	7399 [$R_{int} = 0.0306$]
Absorption correction	Semi-empirical from equiv.	Semi-empirical from equiv.	Semi-empirical from equiv.
Data/restraints/parameters	7254/46/292	7149/4/242	7339/0/291
Goodness-of-fit on F^2	1.025	1.015	1.012
Final *R* indices [$I > 2\sigma(I)$]	$R_1 = 0.0467$, w$R_2 = 0.0888$	$R_1 = 0.0423$, w$R_2 = 0.0812$	$R_1 = 0.0276$, w$R_2 = 0.0528$
R indices (all data)	$R_1 = 0.0663$, w$R_2 = 0.0931$	$R_1 = 0.0558$, w$R_2 = 0.0847$	$R_1 = 0.0351$, w$R_2 = 0.0546$

Compound	**4**	**5**
CCDC deposit no.	271584	271585
Empirical formula	$C_{26}H_{56}Bi_6I_{11}N_4$	$C_{13}H_{30}Bi_3I_{11}N_2O$
Formula weight	4470.43	2253.23
Temperature	150.0(2) K	293(2) K
Crystal system	Triclinic	Monoclinic
Space group	*P*-1	$P2_1/n$
a (Å)	11.9033(6)	17.7008(7)
b (Å)	13.1534(6)	12.6197(5)
c (Å)	15.4462(7)	19.2279(8)
α	97.7210(10)	90
β	109.7160(10)	109.8670(10)
γ	115.5900(10)	90
Volume (Å^3)	1938.37(16)	4039.5(3)
Z	1	4
Density (calculated, Mg/m^3)	3.380	3.705
Absorption coefficient (mm^{-1})	22.352	21.455
F(000)	1904	3848
Crystal size	$0.16 \times 0.12 \times 0.02\,mm^3$	$0.18 \times 0.10 \times 0.06\,mm^3$
Reflections collected	15814	32912
Independent reflections	6836 [$R_{int} = 0.0721$]	7132 [$R_{int} = 0.0472$]
Absorption correction	Semi-emperical from equiv.	Semi-emperical from equiv.
Data/restraints/parameters	6836/0/262	7132/36/212
Goodness-of-fit on F^2	1.019	1.012
Final *R* indices [$I > 2\sigma(I)$]	$R_1 = 0.0495$, w$R_2 = 0.1054$	$R_1 = 0.0340$, w$R_2 = 0.0689$
R indices (all data)	$R_1 = 0.0617$, w$R_2 = 0.1080$	$R_1 = 0.0546$, w$R_2 = 0.0755$

oil. X-ray intensity data covering the full sphere of reciprocal space were measured at 150(2) K (**1**–**4**) or at 293(2) K (**5**) on a Bruker SMART APEX CCD-based diffractometer (Mo$K\alpha$ radiation, $\lambda = 0.71073$ Å) [21,22]. The raw data frames were integrated with SAINT+ [21,22], which also applied corrections for Lorentz and polarization effects. The final unit cell parameters are based on the least-squares refinement of 6046 (**1**), 8586 (**2**), 9971 (**3**), 9397 (**4**), and 8906 (**5**) reflections from the respective data sets with $I > 5(\sigma)I$. Analysis of the data sets showed negligible crystal decay during collection. An empirical absorption correction was applied to each data set using SADABS [21,22]. The structures were solved by a combination of direct methods (**1**, **2**, and **5**) or Patterson methods (**3** and **4**), and difference Fourier syntheses, and refined by full-matrix least squares against F^2 using SHELXTL [23,24]. Descriptions of the structures are given in the Results and Discussions section of this paper. However, noteworthy features of the crystallography experiments are described below. Table 1 contains details of the crystallography experiments for compounds **1**–**5**.

For compound **1**, the asymmetric unit contains one and one-half $[H_2TMDP]^{2+}$ cations in addition to the anion. The 'half-cation' is disordered about an inversion center, and was refined with isotropic displacement parameters only. A total of 46 restraints were used to maintain a reasonable chemical geometry for the disordered cation. All other non-hydrogen atoms were refined with anisotropic displacement parameters; hydrogen atoms were placed in geometrically idealized positions and included as riding atoms.

For compound **2**, an included ethanol molecule of crystallization is disordered equally over two orientations. The disordered EtOH atoms were refined with a common isotropic displacement parameter, with the aid of 4 restraints. All other non-hydrogen atoms were refined with anisotropic displacement parameters. Hydrogen atoms were placed in geometrically idealized positions and included as riding atoms.

Structure solutions of compounds **3** and **4** were routine. For both compounds, all hydrogen atoms on the organic species were clearly observed in the difference maps. However, for the final refinement cycles the hydrogens

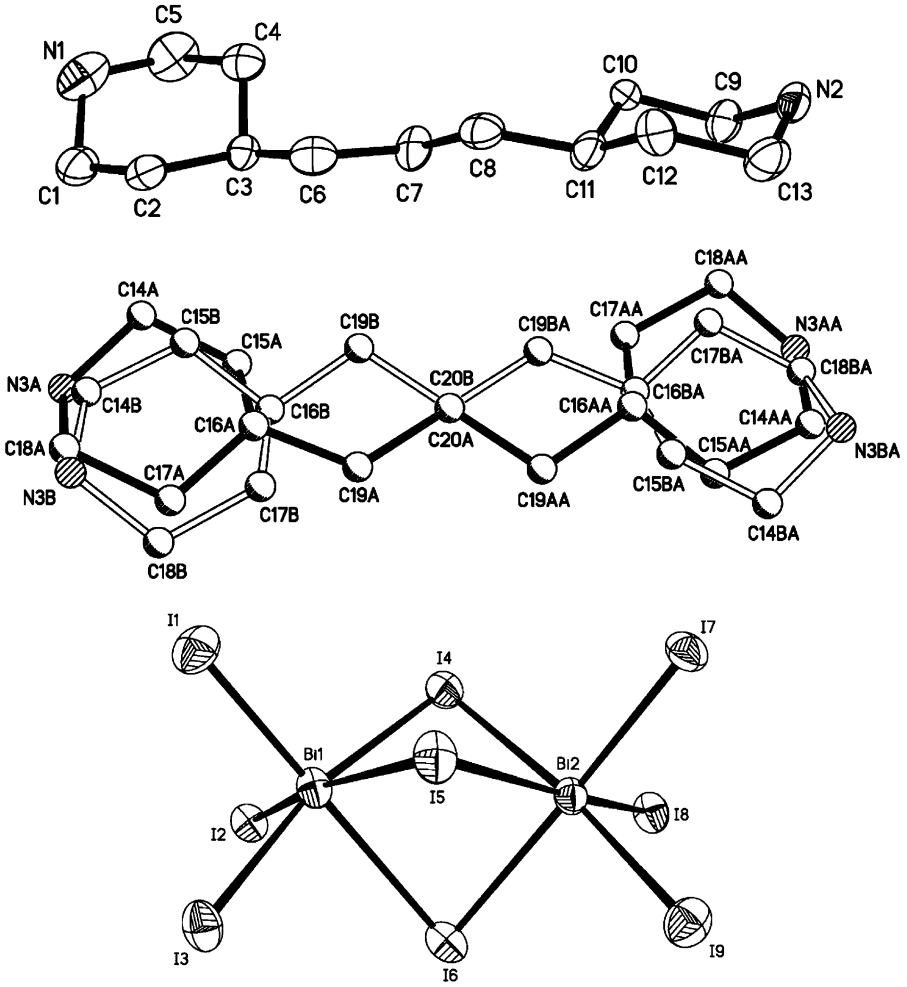

Fig. 1. Thermal ellipsoid plot of the components of **1**. Displacement ellipsoids are shown at the 50% probability level. Both disorder components of the N3A/N3B cation are shown.

were placed in geometrically calculated positions and included with positional and displacement parameters riding on their parent atoms. All non-hydrogen atoms were refined with anisotropic displacement parameters.

For compound **5**, one piperidine ring of the crystallographically independent $[H_2TMDP]^{2+}$ cation is disordered over two orientations in a 50/50 ratio. Atoms of the cation were refined isotropically due to the disorder with the aid of 36 restraints; all other non-hydrogen atoms were refined with anisotropic displacement parameters. Hydrogen atoms of the cation were placed in idealized positions and included as riding atoms; water hydrogens were not located or calculated. Because of this and because of the cation disorder, no attempt was made to identify a hydrogen-bonding network in **5**.

3. Results and discussion

Single crystals of $(H_2TMDP)_3(Bi_2I_9)_2$ (**1**), $(H_2TMDP)_2(Bi_4I_{16})\cdot 2EtOH$ (**2**), $(H_2TMDP)_2(Bi_6I_{22})\cdot 2EtOH$ (**3**), $(H_2TMDP)_2(Bi_6I_{22})$ (**4**), and $(H_2TMDP)(Bi_3I_{11})\cdot H_2O$ (**5**) were all grown solvothermally using ethanol as the reaction solvent. The reaction producing each product involves the in situ formation of an anionic species from the neutral starting material BiI_3. Charge balance for the anion is provided by TMDP, a conformationally flexible organic diamine, which becomes protonated under the specific reaction conditions to yield $[H_2TMDP]^{2+}$. Under the chosen synthesis conditions, the size of the discrete, polynuclear anion formed is found to be dependent upon the relative concentrations of the starting materials in the absence of other factors, such as the presence of an added acid. Generally, it is observed that the size of the anion (in terms of the number of connected bismuth polyhedra) becomes larger as the ratio of BiI_3 to TMDP becomes larger. That is, decreasing the amount of the cation source available for charge balance results in the formation of larger anions. The structures of the specific anions found in compounds **1**–**4** are elaborated upon below along with discussion of the crystal packing arrangement in each compound.

Slightly modifying the synthetic conditions employed to obtain **1**–**4** by introduction of HF as a reagent results in the formation of a polymeric rather than a discrete anionic species. Our previous work has demonstrated that the introduction of additional reagents to the TMDP/BiI_3 system impacts the identity of the anionic species formed in terms of its size, constitution, connectivity, and dimensionality. Specifically, we have observed the formation of a discrete, mixed halide anion when TMDP and BiI_3 are reacted in the presence of HCl under conditions very similar to those employed in the syntheses of **1**–**4**.

Table 2
Hydrogen-bonding interactions in $(H_2TMDP)_3(Bi_2I_9)_2$ (**1**)

D–H···*A*	*d*(D–H)	*d*(H···*A*)	*d*(D···*A*)	<(DHA)
N(1)–H(1N)···I(7)#2	0.92	2.80	3.587(10)	144.5
N(1)–H(2N)···I(7)#3	0.92	2.98	3.775(13)	145.3
N(3A)–H(3A1)···I(6)#3	0.92	2.85	3.63(2)	143.5
N(3A)–H(3A2)···I(3)#3	0.92	2.98	3.76(2)	144.2
N(2)–H(3N)···I(2)#4	0.92	2.92	3.668(9)	139.6
N(2)–H(4N)···I(3)	0.92	2.78	3.675(10)	165.7
N(3B)–H(3B1)···I(6)#5	0.92	3.10	4.01(3)	168.1

Symmetry transformations used to generate equivalent atoms: #1, $-x$, $-y$, $-z$; #2, x, $y-1$, z-1; #3, $-x+1$, $-y$, $-z$; #4, $-x$, $-y+1$, $-z$; #5, x, $y-1$, z.

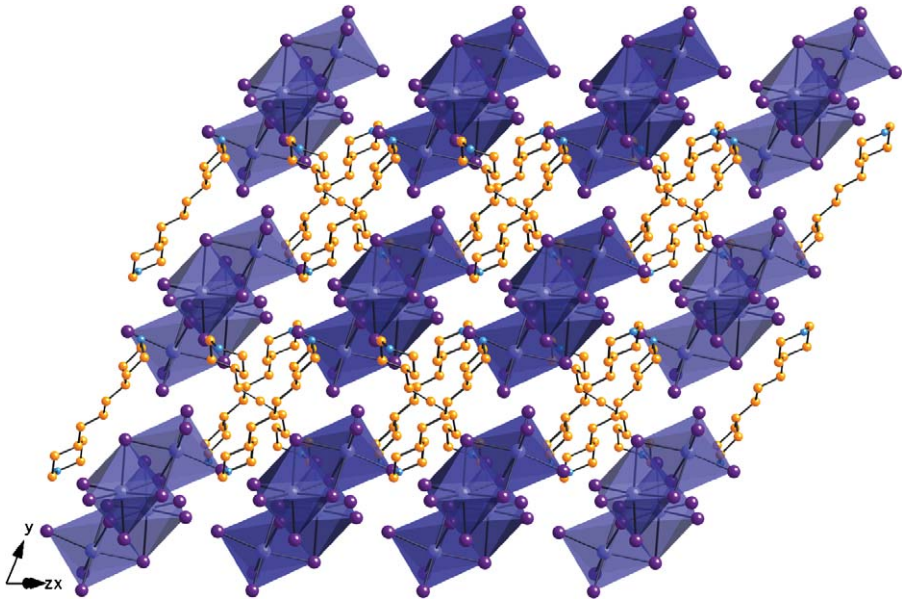

Fig. 2. [101] view of the crystal packing in $(H_2TMDP)_3(Bi_2I_9)_2$. For clarity, only one disorder component of the N3A/N3B cation is shown. Bi polyhedra are shown in blue; I atoms, purple spheres; C atoms, yellow spheres; N atoms, light blue spheres.

Additionally, when HBr is reacted with TMDP and BiI_3, a polymeric, (1-D) mixed halide anionic species is formed [20]. For the TMDP/BiI_3/HF reaction presented here, formation of a mixed halide anionic species is not observed, an observation that is not surprising given that Bi^{3+} is typically regarded as a soft acid and F^- as a hard base. A structural description of the $(Bi_3I_{11})^{2-}$ anion and the crystal packing in $(H_2TMDP)(Bi_3I_{11})\cdot H_2O$ follows.

3.1. Crystal structure of $(H_2TMDP)_3(Bi_2I_9)_2$ (1)

$(H_2TMDP)_3(Bi_2I_9)_2$ crystallizes in the triclinic space group *P*-1. The anionic component of the structure consists of two BiI_6 polyhedra connected in a face-sharing arrangement to produce the $(Bi_2I_9)^{3-}$ anion. The $(Bi_2I_9)^{3-}$ anionic species has been frequently observed in bismuth halide chemistry [1,5,17], and all bond distances and angles of the $(Bi_2I_9)^{3-}$ anion in the present structure are within

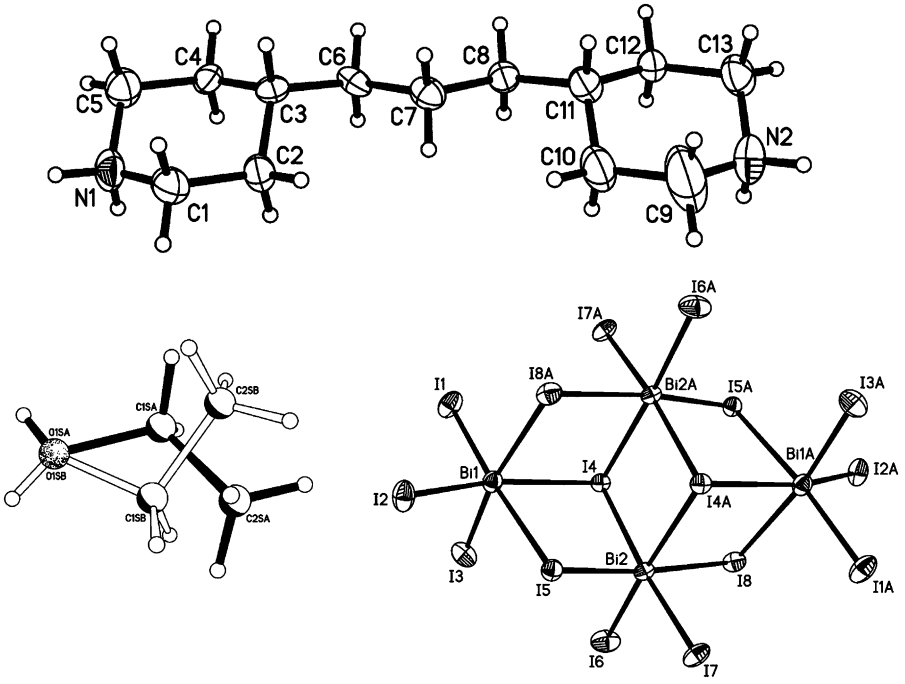

Fig. 3. Thermal ellipsoid plot of the components of **2**. Displacement ellipsoids are drawn at the 50% probability level. Both disorder components of the ethanol molecule of crystallization are shown.

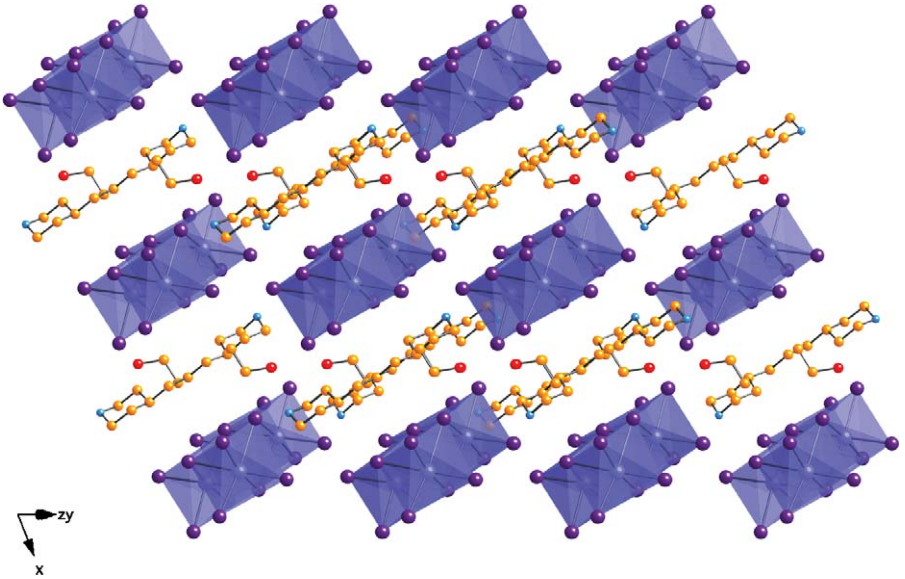

Fig. 4. [011] view of the crystal packing in $(H_2TMDP)_2(Bi_4I_{16})\cdot 2EtOH$. For clarity, only one disorder component of the ethanol solvate molecule is shown. Bi polyhedra are shown in blue; I atoms, purple spheres; C atoms, yellow spheres; N atoms, light blue spheres; O atoms, red spheres.

normal ranges (average Bi–$I_{terminal}$ = 2.973 Å, average Bi-μ_2-I = 3.227 Å). Bond angles in the individual BiI_6 polyhedra deviate from the ideal octahedral angles (*cis* angles range from 80.82(3)° to 97.21(3)°). However, this distortion from ideal is subtle, indicating that the $6s^2$ electron density of bismuth(III) is spherically distributed rather than localized as a lone pair. In addition to the anionic component of the structure, one and one-half protonated $(H_2TMDP)^{2+}$ cations are also present in the asymmetric unit, where the half cation is crystallographically disordered over an inversion center. A thermal ellipsoid plot of the components of **1** is shown in Fig. 1.

Table 3
Hydrogen-bonding interactions in $(H_2TMDP)_2(Bi_4I_{16})\cdot 2EtOH$ (**2**)

D–H···A	d(D–H)	d(H···A)	d(D···A)	<(DHA)
N(1)–H(1A)···I(8)#2	0.92	2.92	3.543(8)	126.0
N(1)–H(1A)···I(7)#2	0.92	3.05	3.697(9)	129.1
O(1SA)–H(1SA)···N(2)#2	0.84	2.12	2.845(17)	144.5
O(1SB)–H(1SB)···I(7)#2	0.84	3.07	3.779(12)	143.1
N(1)–H(1B)···I(8)#1	0.92	2.78	3.678(9)	164.9
N(2)–H(2C)···O(1SA)#3	0.92	1.94	2.845(17)	168.2
N(2)–H(2C)···O(1SB)#3	0.92	1.94	2.845(17)	168.2

Symmetry transformations used to generate equivalent atoms: #1, $-x+1$, $-y+1$, $-z$; #2, x, $y-1$, z; #3, x, $y+1$, z; #4, $-x$, $-y+1$, $-z+1$.

Fig. 2 displays the crystal packing in $(H_2TMDP)_3(Bi_2I_9)_2$. The primary interaction directing the crystal packing is the electrostatic attraction between the cationic and anionic components. However, seven weak N–H···I hydrogen-bonding interactions (Table 2) are also responsible for the observed arrangement of the components in the structure.

3.2. Crystal structure of $(H_2TMDP)_2(Bi_4I_{16})\cdot 2EtOH$ (2)

$(H_2TMDP)_2(Bi_4I_{16})\cdot 2EtOH$ also crystallizes in the triclinic space group *P*-1. The $(Bi_4I_{16})^{4-}$ anion of the structure sits on a crystallographic inversion center; and two crystallographically identical $(H_2TMDP)^{2+}$ cations and two crystallographically identical EtOH solvent molecules complete the asymmetric unit. No disorder is observed in the flexible $(H_2TMDP)^{2+}$ cation; however, the ethanol solvate molecule is crystallographically disordered over two equivalent positions. The $(Bi_4I_{16})^{4-}$ anion consists of two sets of edge-sharing BiI_6 octahedra, and these two edge-sharing bioctahedral units share three edges to produce the centrosymmetric anion. All bond distances and angles of the $(Bi_4I_{16})^{4-}$ anion in the present structure are comparable to those observed in other compounds containing the same anion (average Bi–$I_{terminal}$ = 2.914 Å, average Bi-μ_2-I = 3.225 Å, average Bi-μ_3-I = 3.298 Å);

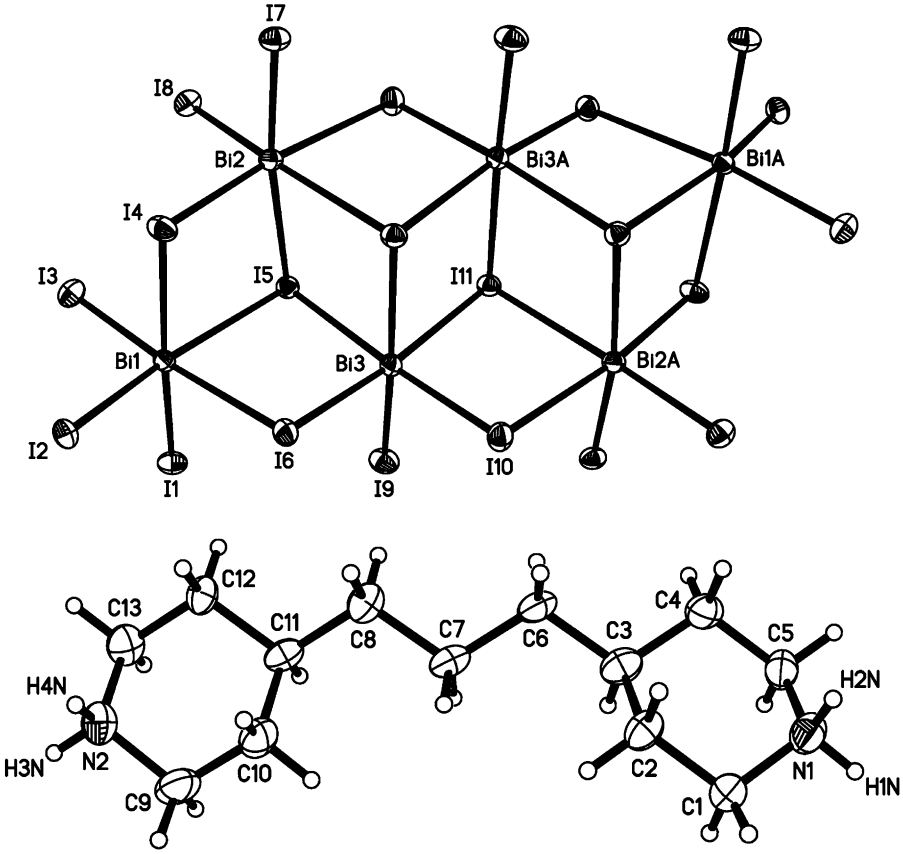

Fig. 5. Thermal ellipsoid plot of the components of **3**. Displacement ellipsoids are drawn at the 50% probability level. The ethanol molecule of crystallization is not shown.

[10,25] and no localization of lone pair electron density on Bi^{3+} is observed in the present structure (*cis* angles range from 80.70(2)° to 99.38(2)°). A thermal ellipsoid plot of the components of **2** is shown in Fig. 3.

Fig. 4 shows the layered crystal packing arrangement of $(H_2TMDP)_2(Bi_4I_{16})\cdot 2EtOH$, where it is observed that the inorganic–organic (211) layers stack in a slightly offset ABAB fashion. In addition to the electrostatic interaction between the bismuth halide anion and the diammonium cation, three N–H···I hydrogen-bonding interactions between cation and anion are also present. Additionally, three cation–solvent hydrogen-bonding interactions (O–H···N) and one anion–solvent hydrogen-bonding interaction (O–H···I) also contribute to the observed crystal packing arrangement (Table 3).

3.3. Crystal structure of $(H_2TMDP)_2(Bi_6I_{22})\cdot 2EtOH$ (**3**)

$(H_2TMDP)_2(Bi_6I_{22})\cdot 2EtOH$ crystallizes in the triclinic space group *P*-1, and the asymmetric unit of the compound consists of half of a centrosymmetric $(Bi_6I_{22})^{4-}$ anion, a $(H_2TMDP)^{2+}$ cation, and an ethanol solvate molecule (Fig. 5). The anion of the structure is constituted of six BiI_6 octahedra, which are connected to one another in an edge-sharing arrangement. Specifically, two sets of three *trans*-edge-sharing octahedra share five edges to produce the centrosymmetric anion. All bond lengths and angles of the anion are comparable to those found in related bismuth

Table 4
Hydrogen-bonding interactions in $(H_2TMDP)_2(Bi_6I_{22})\cdot 2EtOH$ (**3**)

D–H···*A*	*d*(D–H)	*d*(H···*A*)	*d*(D···*A*)	<(DHA)
N(1)–H(1N)···I(7)#2	0.92	2.93	3.628(7)	133.4
N(1)–H(1N)···I(8)#2	0.92	3.06	3.724(7)	130.1
N(1)–H(2N)···I(2)#3	0.92	2.82	3.603(7)	143.7
O(1)–H(1 M)···I(6)	0.90	2.90	3.687(7)	146.9
N(2)–H(3N)···O(1)#4	0.92	1.80	2.721(10)	175.8
N(2)–H(4N)···I(9)#1*	0.92	2.97	3.690(7)	135.9

Symmetry transformations used to generate equivalent atoms: #1, $-x+1$, $-y$, $-z+1$; #2, x, $y+1$, z; #3, $-x+1$, $-y+1$, $-z$; #4, $x+1$, $y-1$, z; *between layers

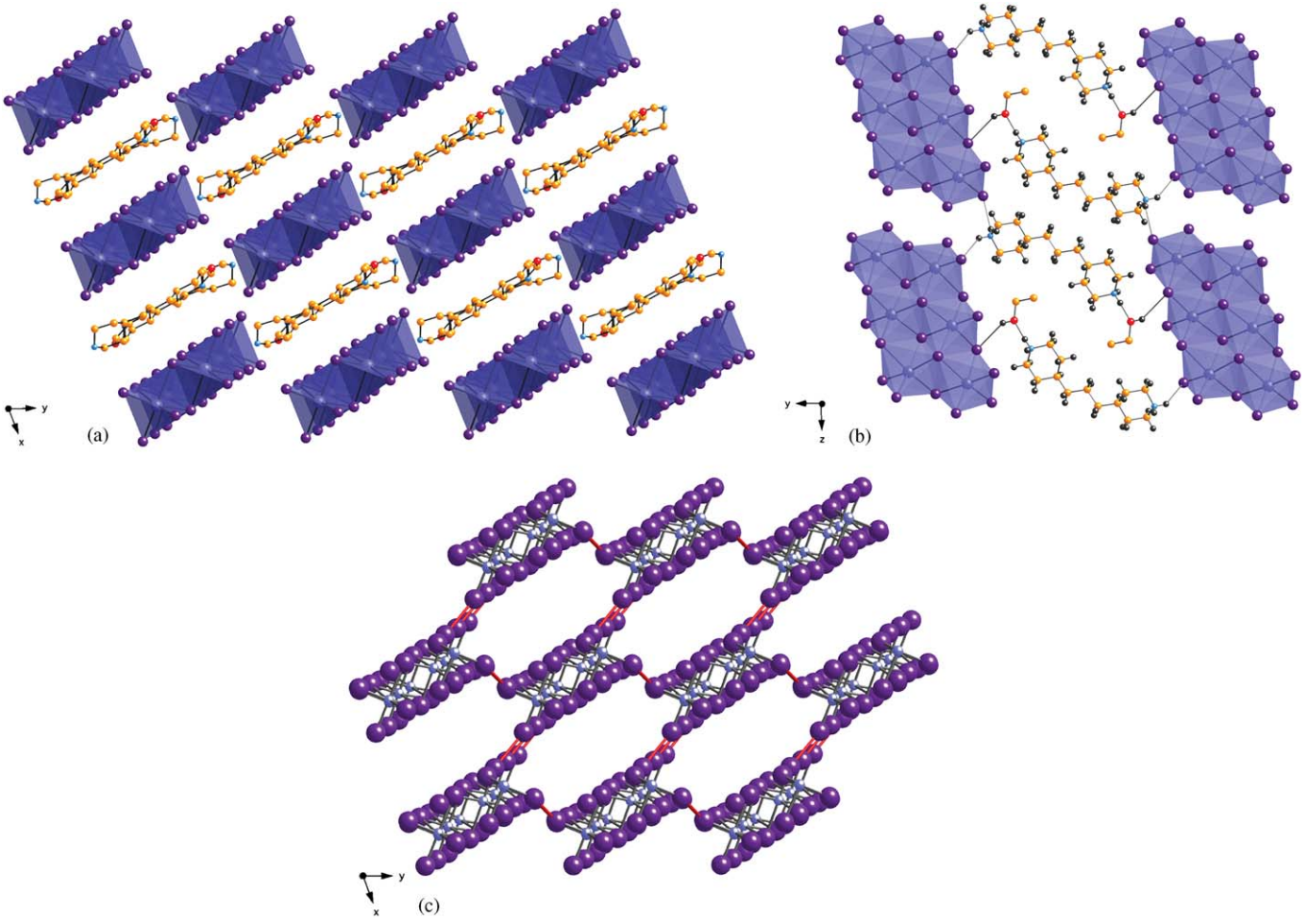

Fig. 6. (a) [001] view of the crystal packing in $(H_2TMDP)_2(Bi_6I_{22})\cdot 2EtOH$. (b) View of a single hydrogen-bonded layer. (c) [001] view (cations/solvent omitted) highlighting the I···I interactions, which connect the anions into a 2-D array. Bi atoms are shown as large blue spheres (blue polyhedra); I atoms, purple spheres; C atoms, yellow spheres; H atoms, grey spheres; N atoms, small, light blue spheres; O atoms, red spheres.

halide-containing compounds (average Bi–$I_{terminal}$ = 2.891 Å, average Bi-μ_2-I = 3.167 Å, average Bi-μ_3-I = 3.290 Å) [14]. However, $(Bi_6I_{22})^{4-}$ has been rarely observed in bismuth halide chemistry [1,13,16]. Bond angles in the BiI_6 polyhedra deviate slightly from the ideal octahedral angles (*cis* angles range from 81.99(2)° to 97.60(2)°), but not significantly enough to indicate localization of the lone pair.

Fig. 6 shows views of the crystal packing in $(H_2TMDP)_2(Bi_6I_{22})\cdot 2EtOH$. Inorganic–organic hybrid layers, stacked in an ABAB fashion, are also observed for compound **3** (Fig. 6a); and cation–anion, anion–solvent, and cation–solvent hydrogen-bonding interactions are observed within these layers (Fig. 6b). Additionally, one N–H$\cdots I$ hydrogen-bonding interaction is present between adjacent layers of the compound (Table 4). Other weak interactions directing the crystal packing in this compound include the $I\cdots I$ interactions between $(Bi_6I_{22})^{4-}$ anions (Fig. 6c). These interactions are brought about by iodine atoms in close proximity to one another, i.e., the distance between the atoms is less than the sum of their van der Waals radii (vdW radius of I = 2.0 Å, $I\cdots I \leqslant 4$ Å) [26]. The $I\cdots I$ interactions present in **3** serve to tether the anions in adjacent layers together into a 2-D array ($I(1)\cdots I(7)$ = 3.944 Å, $I(2)\cdots I(2)$ = 3.813 Å, $I(9)\cdots I(9)$ = 3.923 Å). Overall, the structure can be viewed as a three-dimensional (3-D) connected array when all of the weak interactions (intralayer and interlayer hydrogen-bonding and $I\cdots I$ interactions) are considered.

3.4. Crystal structure of $(H_2TMDP)_2(Bi_6I_{22})$ (4)

Single crystals of $(H_2TMDP)_2(Bi_6I_{22})$ (**4**) co-crystallized from the reaction producing $(H_2TMDP)_2(Bi_6I_{22})\cdot 2EtOH$ (**3**). Compound **4** crystallizes in the triclinic space group *P*-1, and the contents of the asymmetric unit include a full $(H_2TMDP)^{2+}$ cation and half of a centrosymmetric $(Bi_6I_{22})^{4-}$ anion (Fig. 7). The $(Bi_6I_{22})^{4-}$ is the same in compounds **3** and **4** in terms of the connectivity of the polyhedra, the bond lengths (average Bi–$I_{terminal}$ = 2.901 Å, average Bi-μ_2-I = 3.121 Å, average Bi-μ_3-I = 3.299 Å), and the bond angles (*cis* angles range from 83.17(3)° to 98.61(3)°). However, it is worthwhile to point out that the $(H_2TMDP)^{2+}$ cation is conformationally flexible due to its aliphatic spacer and that it adopts different conformations in compounds **3** and **4** (see Figs. 6a and 8a). The conformational flexibility of the cation, along with the absence of EtOH solvate molecules, leads to a different hydrogen-bonding array in compound **4** relative to that observed in compound **3**. In compound **4**, six intralayer

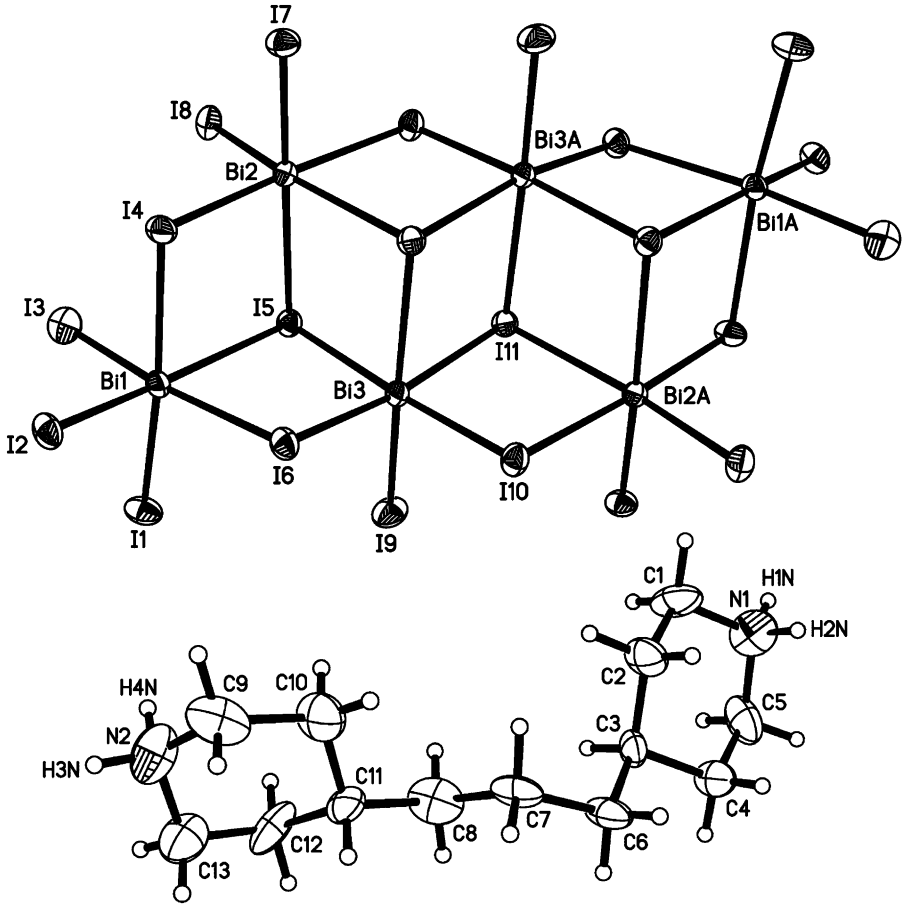

Fig. 7. Thermal ellipsoid plot of the components of **4**. Displacement ellipsoids are drawn at the 50% probability level.

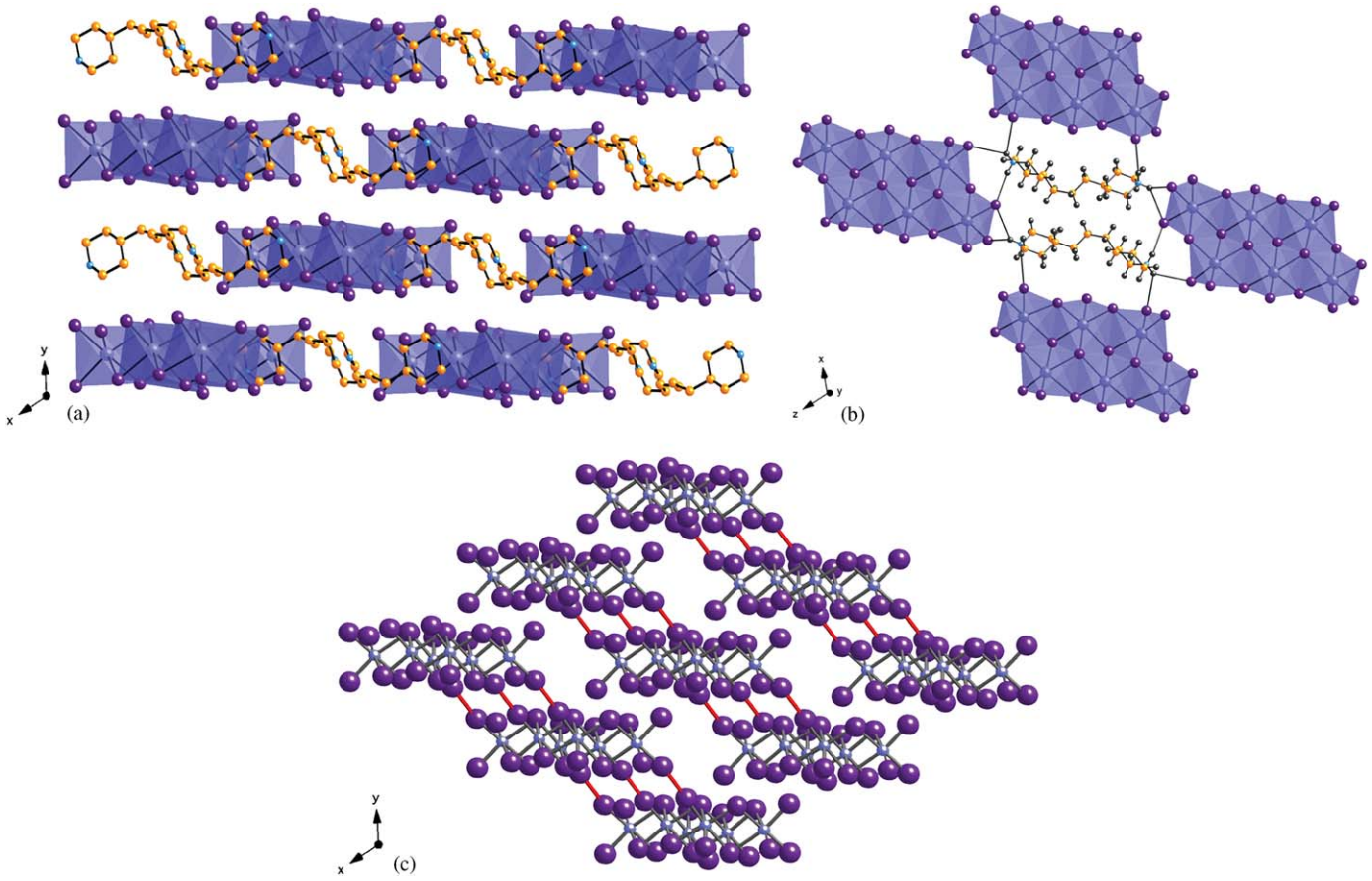

Fig. 8. (a) [001] view of the crystal packing in $(H_2TMDP)_2(Bi_6I_{22})$. (b) View of a single hydrogen-bonded layer. (c) [001] view (cations omitted) highlighting the I···I interactions, which connect the anions into 1-D chains. Bi atoms are shown as large blue spheres (blue polyhedra); I atoms, purple spheres; C atoms, yellow spheres; H atoms, grey spheres; N atoms, small, light blue spheres.

Table 5
Hydrogen-bonding interactions in $(H_2TMDP)_2(Bi_6I_{22})$ (**4**)

D–H···*A*	*d*(D–H)	*d*(H···*A*)	*d*(D···*A*)	<(DHA)
N(1)–H(2N)···I(3)#2	0.92	2.67	3.575(18)	170.3
N(1)–H(1N)···I(7)#3	0.92	2.94	3.638(16)	134.1
N(1)–H(1N)···I(8)#2	0.92	2.98	3.660(16)	131.5
N(2)–H(4N)···I(1)#4	0.92	2.79	3.688(17)	165.1
N(2)–H(3N)···I(3)#5	0.92	3.02	3.691(18)	131.5
N(2)–H(3N)···I(2)#5	0.92	3.03	3.616(17)	123.4

Symmetry transformations used to generate equivalent atoms: #1, $-x+2$, $-y+2$, $-z+1$; #2, $-x+1$, $-y+1$, $-z$; #3, $x-1$, $y-1$, z; #4, $-x+1$, $-y+1$, $-z+1$; #5, $x+1$, y, $z+1$.

hydrogen-bonding interactions are present (Fig. 8b), but there are no hydrogen-bonding interactions present between the layers of the compound (Table 5). However, the hexanuclear anions in neighboring layers are still close enough in space to participate in *I*···*I* interactions between anions (I(1)···I(7) = 3.918 Å, I(9)···I(9) = 3.695 Å), and these interactions connect the anions into 1-D chains (Fig. 8c). Overall, the combination of the weak interactions produces a 3-D connected array of the components in the compound.

3.5. Crystal structure of $(H_2TMDP)(Bi_3I_{11})\cdot H_2O$ (**5**)

$(H_2TMDP)(Bi_3I_{11})\cdot H_2O$ (**5**) crystallizes in the monoclinic space group $P2_1/n$; and contains the polymeric $(Bi_3I_{11})^{2-}$ anion. The asymmetric unit of the compound contains three crystallographically unique Bi atoms and 11 crystallographically unique I atoms of the 1-D polymeric anion in addition to a $(H_2TMDP)^{2+}$ cation and a water molecule. 50/50 disorder of one of the two piperidinium rings of the cation is observed, as shown in Fig. 9.

The $(Bi_3I_{11})^{2-}$ anion of the structure is most conveniently described as consisting of alternating Bi_2I_{10} bioctahedral units and Bi_4I_{16} tetranuclear units, which are connected in an edge-sharing arrangement as shown in Fig. 10a. The Bi_4I_{16} units have the same polyhedral connectivity as the anion of **2**. Alternately, the anion may be described as consisting of Bi_3I_{14} trioctahedral units (three *trans*-edge-sharing BiI_6 octahedra) which share three edges with one neighboring Bi_3I_{14} unit and one edge with another. $(H_2TMDP)(Bi_3I_{11})\cdot H_2O$ represents only the second compound having a polymeric anion of this constitution and connectivity, and the bond lengths and angles of **5** (average Bi–$I_{terminal}$ = 2.895 Å, average

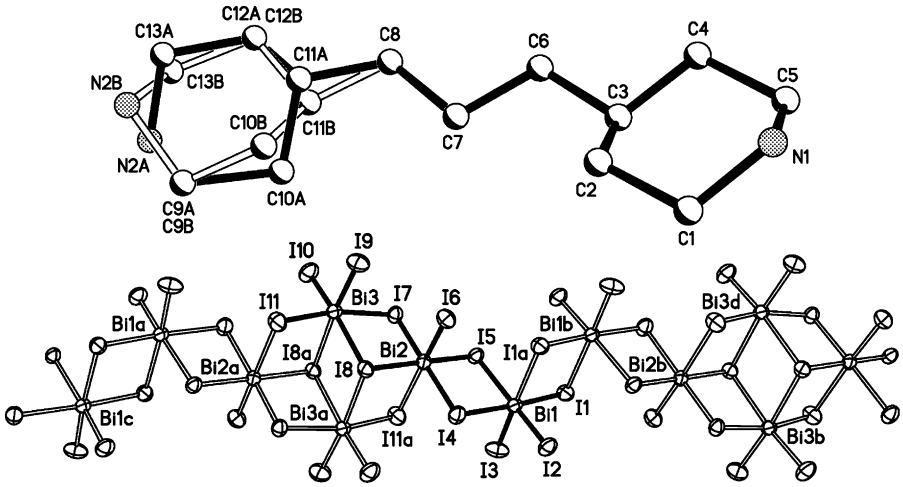

Fig. 9. Thermal ellipsoid plot of the components of **5**. Displacement ellipsoids are drawn at the 50% probability level. For the anion, symmetry unique atoms are connected by dark bonds. For the cation, one piperidine ring is disordered. The water molecule of crystallization is not shown.

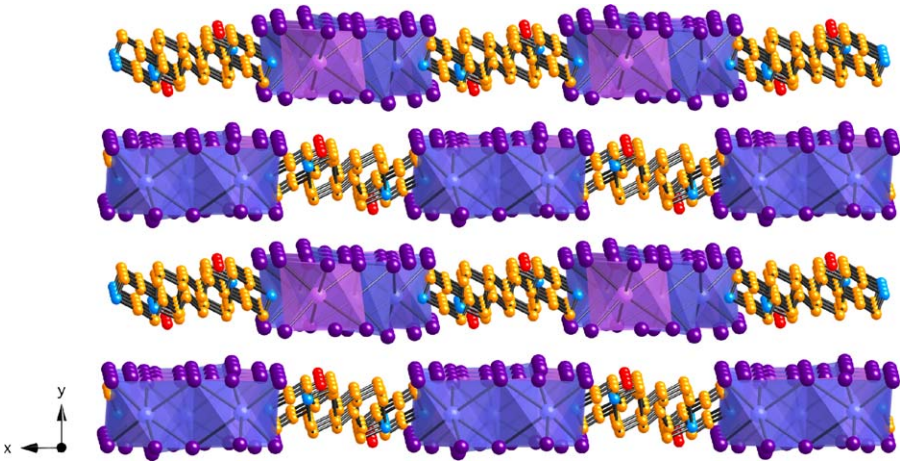

Fig. 10. (a) View of the $(Bi_3I_{11})^{2-}$ anion in **5** highlighting the connectivity of BiI_6 polyhedra. The Bi_4I_{16} tetranuclear cluster is shown in blue and the Bi_2I_{10} bioctahedron is shown in purple. (b) [001] view of the crystal packing. Bi polyhedra are shown in blue and purple; I atoms, purple spheres; C atoms, yellow spheres; N atoms, small, light blue spheres; O atoms, red spheres; H atoms, not shown. For clarity, only one disorder component of the cation is shown.

Bi-μ_2-I = 3.163 Å, average Bi-μ_3-I = 3.316 Å, *cis* angles range from 80.60° to 99.39°) are comparable to those found in $(Et_3PhN)_2(Bi_3I_{11})$ (Et = $-CH_2CH_3$, Ph = $-C_6H_5$), reported earlier [27].

The crystal packing of $(H_2TMDP)(Bi_3I_{11})\cdot H_2O$ is shown in Fig. 10b where it is observed that the infinite 1-D anionic chains of the structure run along the unit cell edges and through the cell center when viewed along [001]. The organic cations of the structure are interleaved between the anionic columns on the unit cell faces. Overall, this arrangement of the components results in inorganic–organic layers when the structure is viewed along [001]. Because the H atoms of the water molecule of crystallization were not calculated or located, no attempt was made to identify a hydrogen-bonding network in the structure. Additionally, no $I\cdots I$ interactions are observed in **5**.

4. Conclusion

Single crystals of five new inorganic–organic salts have been grown solvothermally from BiI_3 and trimethylenedipiperidine hydrate ($TMDP\cdot H_2O$). In the absence of other reagents, it was determined that the size of the inorganic anion increases as the ratio BiI_3:TMDP increases. While mixed halide anions of bismuth(III) have been observed upon introduction of a haloacid (HCl or HBr) to the TMDP/BiI_3 system, a polymeric iodobismuthate anion is observed to be the product upon addition of HF. Thus, it was determined that the identity of the halobismuthate anion, in terms of the number, constitution, and connectivity of BiX_6 polyhedra, is heavily tied to the specific reaction conditions. Consequently, it is conceivable that a great number of halobismuthate anions may be synthesized, and that compounds containing such anions may be

ideal systems for the study of interesting physical phenomena, such as size dependent optical properties and low-dimensional semiconductivity.

5. Supporting information

CCDC-271581-85 contain the supplementary crystallographic data for this paper. These data can be obtained free of charge at www.ccdc.cam.ac.uk/conts/retrieving.html [or from the Cambridge Crystallographic Data Centre (CCDC), 12 Union Road, Cambridge CB2 1EZ, UK; fax: +44(0)1223-336033; *E-mail*: deposit@ccdc.cam.ac.uk].

Acknowledgments

Financial support of this project was provided by the National Science Foundation through grant numbers CHE:0314164 and CHE:0315152.

References

[1] H. Eickmeier, B. Jaschinski, A. Hepp, J. Nuß, H. Reuter, R. Blachnik, Z. Naturforsch. Teil B 54 (1999) 305.
[2] D.B. Mitzi, P. Brock, Inorg. Chem. 40 (2001) 2096.
[3] G.A. Mousdis, G.C. Papavassiliou, A. Terzis, C.P. Raptopoulou, Z. Naturforsch. Teil B 53 (1998) 927.
[4] G.C. Papavassiliou, I.B. Koutselas, A. Terzis, C.P. Raptopoulou, Z. Naturforsch. Teil B 50 (1995) 1566.
[5] X.-H. Zhu, N. Mercier, P. Frère, P. Blanchard, J. Roncali, M. Allain, C. Pasquier, A. Riou, Inorg. Chem. 42 (2003) 5330.
[6] J.M. Ryan, Z. Xu, Inorg. Chem. 43 (2004) 4106.
[7] D.B. Mitzi, Inorg. Chem. 39 (2000) 6107.
[8] Z. Xu, D.B. Mitzi, Inorg. Chem. 42 (2003) 6589.
[9] C.J. Carmalt, L.J. Farrugia, N.C. Norman, Z. Anorg. Allg. Chem. 621 (1995) 47.
[10] C.J. Carmalt, L.J. Farrugia, N.C. Norman, Z. Naturforsch. Teil B 50 (1995) 1591.
[11] A.M. Goforth, J.R. Gardinier, M.D. Smith, J. Peterson, L.H.-C. zur Loye, Inorg. Chem. Commun. 8 (2005) 684.
[12] M. Lindsjo, A. Fischer, L. Kloo, Z. Anorg. Allg. Chem. 631 (2005) 1497.
[13] H. Krautscheid, Z. Anorg. Allg. Chem. 620 (1994) 1559.
[14] C. Feldmann, J. Solid State Chem. 172 (2003) 53.
[15] A. Cornia, A.C. Fabretti, R. Grandi, W. Malavasi, J. Chem. Crystallogr. 24 (1994) 277.
[16] W. Clegg, R.J. Errington, G.A. Fisher, M.E. Green, D.C.R. Hockless, N.C. Norman, Chem. Ber. 124 (1991) 2457.
[17] F. Lazarini, Acta Crystallogr. Sect. C 43 (1987) 875.
[18] U. Geiser, E. Wade, H.H. Wang, J.M. Williams, Acta Crystallogr. Sect. C 46 (1990) 1547.
[19] S. Chaabouni, S. Kamoun, J. Jaud, J. Chem. Crystallogr. 27 (1997) 527.
[20] A.M. Goforth, M.D. Smith, L. Peterson, Jr., H.-C. zur Loye, Inorg. Chem. 43 (2004) 7042.
[21] SMART Version 5.625, SAINT+ Version 6.02a and SADABS, Bruker Analytical X-ray Systems, Inc, Madison, WI, USA, 1998.
[22] SMART Version 5.628, SAINT+ Version 6.22 and SADABS Version 2.05, Bruker Analytical X-ray Systems, Inc., Madison, WI, USA, 2001.
[23] G.M. Sheldrick, SHELXTL Version 5.1, Bruker Analytical X-ray Systems, Inc., Madison, WI, USA, 1997.
[24] G.M. Sheldrick, SHELXTL Version 6.1, Bruker Analytical X-ray Systems, Inc., Madison, WI, USA, 2000.
[25] R. Kubiak, K. Ejsmont, J. Mol. Struct. 474 (1999) 275.
[26] A. Bondi, J. Phys. Chem. 68 (1964) 441.
[27] H. Krautscheid, Z. Anorg. Allg. Chem. 621 (1995) 2049.